

1 A honeycomb seafloor morphology in carbonate sediment  
2 of the Carnegie Ridge (offshore Ecuador): Formation and  
3 potential geodynamic significance

4 F. Michaud<sup>1,2\*</sup>, J.Y. Collot<sup>1</sup>, G. Ratzov<sup>1</sup>, J.N. Proust<sup>3</sup>, A. Dano<sup>1</sup>, J.F. Lebrun<sup>4</sup>, M.J.  
5 Hernández<sup>1,5,6</sup>, G. Loayza<sup>7</sup>, A. Khaoulani<sup>1</sup>, Y. Stoll<sup>1</sup>, H. Pouderoux<sup>3</sup>, and L. De Min<sup>4</sup>

6 <sup>1</sup> Université Côte d'Azur, IRD (Institut de Recherche pour le Développement), Sorbonne  
7 Université, CNRS (Centre National de la Recherche Scientifique), Observatoire de la  
8 Côte d'Azur, GEOAZUR (laboratoire de Géoazur), 06560 Valbonne, France

9 <sup>2</sup> Sorbonne Université, Faculté des Sciences et Ingénierie, F-75252 Paris, France

10 <sup>3</sup> CNRS, OSUR (Observatoire des Sciences de l'Univers de Rennes), Géosciences  
11 Rennes, Université de Rennes, 35042 Rennes, France

12 <sup>4</sup> Université des Antilles et de la Guyane, Département de Géologie, Pointe à Pitre  
13 97157, France

14 <sup>5</sup> Sorbonne Université, Institut des Sciences de la Terre de Paris (ISTeP), Campus Pierre  
15 et Marie Curie, 75252 Paris, France

16 <sup>6</sup> Departamento de Geología, Escuela Politécnica Nacional, Quito, Ecuador

17 <sup>7</sup> Escuela Superior Politécnica del Litoral, Guayaquil, Ecuador

18

19 \*E-mail: micho@geoazur.unice.fr

20

21 **ABSTRACT**

22 Based on swath bathymetry, two-dimensional, high-resolution seismic reflection profiles,  
23 and Ocean Drilling Program/Deep Sea Drilling Project (ODP/DSDP) data, we describe a  
24 seafloor honeycomb pattern and propose a model for its formation in Pliocene–Miocene

carbonate deposited on the uneven oceanic basement of the Carnegie Ridge (offshore Ecuador). Hydrothermal fluids derived from the basement aquifer fractured and dissolved carbonate sediment, creating seafloor pits above basements highs. Fluids expelled along polygonal faults may have assisted the nucleation of seafloor depressions. At the Pliocene-Pleistocene boundary, strong bottom currents scoured previously damaged sediments, enlarging the initial depressions and producing the seafloor honeycomb pattern. This regional erosive episode was contemporaneous with the final closing of the Isthmus of Panama and the clogging of the Ecuador Trench by the subduction of the Carnegie Ridge, so that the honeycomb pattern may be viewed as a regional marker of these two geodynamic events.

## INTRODUCTION

Only a few cases of kilometer-scale honeycomb pattern (HP) on the seafloor have been reported along continental margins and generally into siliceous or mudstone-dominated sediments. The main examples are (1) kilometer-scale seabed high-centered polygons (Berndt et al., 2012) outlined by 20-m-deep, elongated pockmarks, formed by sediment contraction related to fluid circulation along polygonal faults; and (2) polygonal crests separating hectometer- to kilometer-scale, 60-m-deep depressions formed by long-term unstable bottom currents (Sun et al., 2017). Here, we used new multibeam data collected during the 2012 ATACAMES cruise (RV L'Atalante) on the Carnegie Ridge offshore Ecuador (<http://campagnes.flotteoceanographique.fr/campagnes/12010010/>; Fig. 1) to report, for the first time, a HP morphology in carbonate sediment.

The HP consists of a network of kilometer-scale, hectometer-deep, polygonal depressions (Figs. 2 and 3). Based on a low-resolution bathymetric data set, the depressions were initially reported as densely packed subcircular features (Michaud et al., 2005). The ATACAMES high-resolution multibeam data and seismic profiles (72 tracks, 50–450 Hz) allow the nature of the polygonal depressions to be investigated. We present a coherent model for their formation in relation to sedimentation, fluid circulation, and large-scale seafloor erosion. Additionally, we discuss the timing, the origin, and the widespread distribution of the HP in relation to the closing of the Isthmus of Panama and subduction of the Carnegie Ridge.

## **CARNEGIE RIDGE FRAMEWORK**

The interplay of the Galapagos hotspot with the Cocos-Nazca spreading center led to the formation of the Cocos, Malpelo, and Carnegie Ridges (Fig. 1A; Lonsdale and Klitgord, 1978). Deep Sea Drilling Project (DSDP) Site 157 (van Andel et al., 1973), and Ocean Drilling Program (ODP) Sites 1238 and 1239 (Fig. 1B; Mix et al., 2003) reveal a 400–500-m-thick Miocene to Pleistocene carbonate sediment cover over the oceanic basement. Two lithologic units were defined at Sites 157 and 1238, an upper unit, consisting of ~300 m of oozes and chalk, and a lower unit, composed of ~100 m of lithified interbedded chalk and chert horizons (Fig. DR1 in the GSA Data Repository<sup>1</sup>). Subcircular depressions fields are present on the Carnegie, Cocos, and Malpelo Ridges (Fig. 1A), and they have been globally attributed to regional submarine carbonate dissolution processes enhanced by bottom currents (Lonsdale and Fornari, 1980).

## **DEPRESSION GEOMETRIES**

The seafloor depressions of the HP area are typically 0.8–2.0 km wide, separated by 100–250 m high, dominantly linear ridges (supplemental information Table 1) (Fig.2, 3, and Fig.S2). The ridges give the depressions their polygonal and, by places, hexagonal shape, and enclose sub-circular depression bottoms (Fig.3). Most polygonal depressions lay in 2100-2800 m of water depth together with isolated, sub-circular to ovoid, larger depressions (3-4 km-wide and 400 m-deep) (Fig.2); the largest being located deeper than 2500 m.

## **ACOUSTIC BASEMENT AND FEATURES OF SEDIMENTARY COVER UNITS**

### **Acoustic Basement**

The acoustic basement is marked by a set of strong and chaotic reflections (Fig. 4) overlain by a thinly laminated sedimentary cover 0.4–0.8 s two-way traveltime (TWTT) in thickness. The basement shows a remarkable step that is 0.8 s TWTT high and trends east-west in map view (Figs. 2 and 4). South of the step, the acoustic basement is smooth and lies at a 4.3–4.5 s TWTT in depth; the sediment is 0.8 s TWTT thick, locally carved by isolated depressions and moats (Fig. 2). North of the step, the acoustic basement is shallower and locally crops out at the seafloor (stars on Fig. 4B). When probed by seismic data (Fig. 2), the depressions were observed to have preferentially (73%) developed where the acoustic basement is rough (Table DR1). However, where the acoustic basement is smooth, some lows filled with sediment represent channel-fill structures (Fig. 4A, profile ATAC129, zoom1). In the sedimentary cover, we

differentiated a lower unit, u1, from an upper unit, u2 (Fig. 4), separated by a major erosional unconformity.

#### **Lower Unit u1**

The lower unit u1 (Fig. 4A) returns subparallel continuous reflectors. Unit u1 extends over the entire region, including the acoustic basement step, but it is absent in some depressions. The base of u1 locally shows a thin transparent or poorly reflective layer (Fig. 4A, profile ATAC129, zoom1). South of the basement step, u1 is 0.6 s TWTT thick. There, the poorly reflective lower half of u1 is bounded at the top by a dome-shaped reflector crossing the original subparallel reflectors (Fig. 4A, Common Depth Point [CDP] 5000–7000; Fig. DR3, profile ATAC131 CDP 1000– 2500). This dome-shaped reflector suggests that a diagenetic front rose in the sediment cover crossing the original strata. To the north of the step, the thickness of u1 varies from 0 to 0.6 s TWTT further north along profile ATAC126 (Fig. 4B). An undulating geometry showing locally internal cutand- fill structures characterizes the unit above the rough basement area (Fig. 4B, zoom2 and zoom3; Fig. 4A, profile ATAC130, CDP 2000–4000), suggesting a sediment drift pattern (Faugeres et al., 1999).

The major unconformity truncates u1 in the buried depressions (Fig. 4A, ATAC129, CDP 1000–3000, zoom1; Fig. 4B, zoom2), and at the walls of most of the seafloor depressions (Fig. 4A, CDP 3600–4000, zoom2; Fig. 4B, CDP 15800–16500). In cross section, this erosional surface outlines the triangular shape of the ridges between the polygonal depressions carved into u1 (Fig. 4B, zoom2 and zoom3).

Normal faults with 5- to 20-m-scale vertical offsets (red arrows in Figs. 4A and 4B, zoom1 and zoom4) deform u1. Most of them show characteristics of polygonal faults

(Gay et al., 2004) as they disappear upward and downward, do not end at a specific horizon, show a low frequency in lateral distribution, and may link up in polygons in plan view, as demonstrated in other parts of the world where three-dimensional (3-D) seismic control is available (Cartwright et al., 2003).

Although time migration with a constant 1500 m/s velocity produced clear seismic imaging, imperfect migration velocities led to poor seismic imaging, preventing local geological interpretation. Indeed, only vertical acoustic anomalies associated with well-collapsed diffractions in u1 (Fig. 4A, zoom1 and zoom4) are interpreted as fluid-escape pipes (Cartwright and Santamarina, 2015).

## **Upper Unit u2**

The upper unit u2 is thinly stratified and discontinuous, and its thickness varies from 0 in some depressions to 0.4 s TWTT south of the basement step. Although locally concordant with u1 (Fig. 4A, CDP 5000–7000; Fig. 4B, CDP 2000–4000), unit u2 unconformably overlies (Fig. 4, zoom1, zoom2, and zoom3) the erosional topographies carved in u1. Unit u2 shows internal discontinuities and undulating depositional patterns pointing to sediment drift (Fig. 4A, zoom1) and exhibits complex migration and aggradation geometries, especially in the rough acoustic basement areas (Fig. 4B, zoom2, 3; Fig. DR3, ATAC128 CDP 7000–8500, ATAC131 CDP 5000–7500). These geometries resemble contourite drifts produced by the interaction between oceanic bottom currents and the seafloor topography.

## **DISCUSSION**

### **Origin of The Honeycomb Seafloor Morphology**

A similar kilometer-scale, seafloor HP was previously interpreted to originate from smaller counterparts developed in underlying sedimentary units as a result of a sediment drift depositional pattern (Sun et al., 2017). This pattern is characterized by wave-like geometries corresponding to cut-and-fill erosional features with honeycomb planforms. It was attributed to the action of unsteady bottom currents initiated in the late Miocene in the South China Sea. In our study area, without 3-D seismic data, the HP seafloor cannot be demonstrated to mimic buried honeycomb structures. Nevertheless, this hypothesis is not ruled out, as unit u1 exhibits wave-like geometry where the acoustic basement is rough (zoom2, and basement step along profile ATAC130 in Fig. 4), and depression 3 (Fig. 4B) shows that unit u2 sediment drift filled up a polygonal depression carved in u1, reproducing the underlying honeycomb pattern. Many polygonal depressions (Fig. 3A) carved into u1 (Fig. 4B, zoom2 and zoom3) are, however, deeper (~200–300 m) than those (~60 m) described by Sun et al. (2017), suggesting that other important processes are involved.

Polygonal faults generally form in mud-rich sediment (Cartwright et al., 2003) by dewatering and, among other processes (Goult, 2008), by differential compaction of the host sediment (Berndt et al., 2012) related, to either sediment thickness variations (zoom4, Fig. 4; Mayer, 1981) or silica diagenesis (Davies and Ireland, 2011). On the Carnegie Ridge, in the areas where we interpret a diagenetic front (Fig. 4A, CDP 4800–5500; Fig. DR3, ATAC131, CDP 2000–2500), u1 reflectors and the seafloor draw an elongated depression controlled by normal faults, likely relating to diagenesis conversion. Indeed, according to DSDP Leg 16 and ODP Leg 202, the sedimentary cover of the Carnegie and Cocos Ridges is dominantly composed of carbonate, but the sediment close

to the basement reveals chert and micrite, indicating significant opal and carbonate diagenesis (Mix et al., 2003; Moore, 2008). Consequently, a polygonal fault network is expected in the studied HP area. According to Gay et al. (2004), furrows are initially produced at the seafloor along polygonal faults, with pockmarks developing above high-drainage chimneys at the triple junction of three adjacent hexagonal cells (Figs. 5A and 5C). In a carbonate environment, Moore et al. (2007) showed that hydrothermal discharge contributes to sediment fracture and damage, creating pits over oceanic basement highs (Figs. 5B and 5D). Based on a mass balance analysis, Bekins et al. (2007) indicated that the formation of pits in the equatorial Pacific could have been enhanced by dissolution of carbonate sediment by fluids undersaturated with calcite exiting basement vents. Fluids are therefore considered as a key factor in the initiation of seafloor depressions on the Carnegie Ridge.

Subsequently, the pockmarks and pits were enlarged and deepened in response to the action of strong bottom currents (Sun et al., 2011), shaping the regional unconformity between u1 and u2 (Lonsdale and Malfait, 1974). The currents preferentially removed sediments weakened by fracturing and fluid circulation, scouring depressions down to the indurated base of u1, or to the top of the oceanic basement (Fig. 5E). In the pit case, the currents action allowed the pit to grow radially, leaving at the end a polygonal depression pattern. In the pockmark case, the impact of current scouring is uneven, because it is controlled by the current direction with respect to the orientation of the hexagonal cell pattern. Indeed, triple junctions of adjacent cells offer both convergent and divergent (Fig. 5A) geometries for current action. The current is funneled and accelerated by the convergent geometry, so that erosion is locally enhanced, initiating subcircular



depressions at every other triple junction. This process allows the pockmarks to grow in diameter, leaving at the end an HP that is offset laterally by a half-hexagonal cell with respect to the initial polygonal fault network. Many depressions show elongated or free shapes locally crossed by minor ridges (Fig. 3B) due to irregular basement topography, and partial or full erosion of some interdepression ridges. At the end, u2 sediment drift is plastered against the wall of some polygonal depressions carved in u1 (Fig. 5F).

#### **Possible Regional Cause for the Scouring of the HP**

Seismic records collected near DSDP Site 157 (Fig. 1B; Heath and van Andel, 1973; van Andel et al., 1973) show several unconformities in the upper 110–125 m of Pleistocene sediment. DSDP Site 157 drilled u2 immediately west of our study zone (Fig. 1B) and recovered 116 m of Pleistocene sediment above the Pliocene sequence (Fig. DR1). On profile ATAC126, u2 is ~80 m thick (Fig. 4B, CDP 2000–4500) and could then include the entire Pleistocene sequence drilled at DSDP Site 157. Consequently, the highly erosive episode that we associate with new current conditions is likely to have started at the transition between Pliocene and Pleistocene times.

At a regional scale, DSDP Site 158 (Fig. 1A), drilled on the Cocos Ridge, revealed a shallow hiatus covering most of the late Pliocene (Heath and van Andel, 1973). Further northeast along the Cocos Ridge, ODP Site 1242 (Fig. 1A) shows a major unconformity (Mix et al., 2003) and a hiatus that encompasses the interval from 13 to 2.5 Ma. On the Malpelo Ridge, kilometer- scale erosional depressions were initiated during the mid-Pliocene (Lonsdale and Fornari, 1980). If the origin and the age of the depression fields

on the Carnegie, Cocos, and Malpelo Ridges are identical to those proposed in this study, the erosive episode appears to be of regional extent.

Major changes in the configuration of ocean gateway and related deep currents are triggered by geodynamic events (Moore et al., 2004). The formation of the Isthmus of Panama stands as one of the greatest geological events driving profound transformations in ocean circulation. The collision of the Carnegie Ridge with the South American margin clogged the subduction trench, contributing, together with the gradually emerging land of Panama, to the enclosure of the Panama Basin, and to the change in the regional bottom current configuration (Lonsdale and Fornari, 1980).

In a review, O'Dea et al. (2016) dated the emergence of the Isthmus of Panama at 2.8 Ma, close to the inferred age for the beginning of the current- driven, erosive regional episode observed on the Carnegie Ridge that carved and partially filled the honeycomb polygonal depression network.

In conclusion, polygonal faults, which are globally scarce in the studied carbonate ooze environment, were not clearly imaged in the HP area, possibly because they disappeared during the scouring process, as suggested in our model. In contrast, seafloor polygonal depressions statistically correlate with the rough basement topography. Hydrothermal fluid circulation and dissolution affecting the carbonate sediment overlying the rough oceanic basement provide support for the pit origin of the depressions. Strong bottom currents acting at the Pliocene-Pleistocene boundary, possibly as a result of the closure of the Isthmus of Panama, were instrumental in scouring the polygonal depressions.

## ACKNOWLEDGMENTS

We thank the crew of R/V L'Atalante and GENAVIR. This work was supported by Institut National des Sciences de l'Univers (INSU) du Centre National de la Recherche Scientifique (CNRS). Thanks to Institut de la Recherche et du Développement (IRD), to Instituto Oceanográfico de la Armada (INOCAR) and Ministry of Higher Education, Science, Technology and Innovation of Ecuador (SENESCYT).

## REFERENCES CITED

- Bekins, B.A., Spivack, A.J., Davis, E.E., and Mayer, L.A., 2007, Dissolution of biogenic ooze over basement edifices in the equatorial Pacific with implications for hydrothermal ventilation of the oceanic crust: *Geology*, v. 35, p. 679–682, <https://doi.org/10.1130/G23797A.1>.
- Berndt, C., Jacobs, C., Evans, A., Gay, A., Elliott, G., Long, D., and Hitchen, K., 2012, Kilometre-scale polygonal seabed depressions in the Hatton Basin, NE Atlantic Ocean: Constraints on the origin of polygonal faulting: *Marine Geology*, v. 332–334, p. 126–133, <https://doi.org/10.1016/j.margeo.2012.09.013>.
- Cartwright, J.A., and Santamarina, C., 2015, Seismic characteristics of fluid escape pipes in sedimentary basins: Implications for pipe genesis: *Marine and Petroleum Geology*, v. 65, p. 126–140, <https://doi.org/10.1016/j.marpetgeo.2015.03.023>.
- Cartwright, J.A., James, D., and Bolton, A., 2003, The genesis of polygonal fault systems: A review, *in* Van Rensbergen, P., et al., eds., *Subsurface Sediment Mobilization*: Geological Society London Special Publication 216, p. 223–243, <https://doi.org/10.1144/GSL.SP.2003.216.01.15>.

255 Davies, R.J., and Ireland, M.T., 2011, Initiation and propagation of polygonal fault arrays  
 256 by thermally triggered volume reduction reactions in siliceous sediment: *Marine*  
 257 *Geology*, v. 289, p. 150–158, <https://doi.org/10.1016/j.margeo.2011.05.005>.  
 258 Faugères, J.C., Stow, D.A.V., Imbert, P., and Viana, A., 1999, Seismic features  
 259 diagnostic of contourite drifts: *Marine Geology*, v. 162, p. 1–38,  
 260 [https://doi.org/10.1016/S0025-3227\(99\)00068-7](https://doi.org/10.1016/S0025-3227(99)00068-7).  
 261 Gay, A., Lopez, M., Cochonat, P., and Sermondadaz, G., 2004, G. Polygonal faults  
 262 furrows system related to early stages of compaction Upper Miocene to recent  
 263 sediments of the Lower Congo Basin: *Basin Research*, v. 16, p. 101–116,  
 264 <https://doi.org/10.1111/j.1365-2117.2003.00224.x>.  
 265 Goult, N. R., 2008, Geomechanics of polygonal fault systems: a review: *Petroleum*  
 266 *Geoscience*, 14, p. 389–397.  
 267 Heath, G.R., and van Andel, T.H., 1973, Tectonics and sedimentation in the Panama  
 268 basin: Geological results of Leg 16, *in* van Andel, T.H., and Heath, G.R., eds., *Initial*  
 269 *Reports of the Deep Sea Drilling Project, Volume 16*: Washington, D.C., U.S.  
 270 Government Printing Office, p. 899–913.  
 271 Lonsdale, P., and Fornari, D., 1980, Submarine Geology of the Malpelo Ridge, Panama  
 272 Basin: *Marine Geology*, v. 36, p. 65–83, [https://doi.org/10.1016/0025-](https://doi.org/10.1016/0025-3227(80)90041-9)  
 273 [3227\(80\)90041-9](https://doi.org/10.1016/0025-3227(80)90041-9).  
 274 Lonsdale, P., and Klitgord, K.D., 1978, Structure and tectonic history of the eastern  
 275 Panama Basin: *Geological Society of America Bulletin*, v. 89, p. 981–999,  
 276 [https://doi.org/10.1130/0016-7606\(1978\)89<981:SATHOT>2.0.CO;2](https://doi.org/10.1130/0016-7606(1978)89<981:SATHOT>2.0.CO;2).

277 Lonsdale, P., and Malfait, B.T., 1974, Abyssal dunes of foraminiferal sand on the  
 278 Carnegie Ridge: Geological Society of America Bulletin, v. 85, p. 1697–1712,  
 279 [https://doi.org/10.1130/0016-7606\(1974\)85<1697:ADOFSO>2.0.CO;2](https://doi.org/10.1130/0016-7606(1974)85<1697:ADOFSO>2.0.CO;2).  
 280 Mayer, L., 1981, Erosional troughs in deep-sea carbonates and their relationship to  
 281 basement structure: Marine Geology, v. 39, p. 59–80, [https://doi.org/10.1016/0025-  
 282 3227\(81\)90028-1](https://doi.org/10.1016/0025-3227(81)90028-1).  
 283 Michaud, F., Chabert, A., Collot, J.Y., Sallarès, V., Flueh, E.R., Charvis, P., Graindorge,  
 284 D., Gustcher, M.A., and Bialas, J., 2005, Fields of multi-kilometer scale sub-circular  
 285 depressions in the Carnegie ridge sedimentary blanket: effect of underwater  
 286 carbonate dissolution?: Marine Geology, v. 216, p. 205–219,  
 287 <https://doi.org/10.1016/j.margeo.2005.01.003>.  
 288 Mix, A.C., Tiedemann, R., Blum, P., et al., 2003, Proceedings of the Ocean Drilling  
 289 Program Initial Reports, 202: College Station, Texas, Ocean Drilling Program, 145  
 290 p., doi:10.2973/odp.proc.ir.202.2003.  
 291 Moore, T.C., 2008, Chert in the Pacific: Biogenic silica and hydrothermal circulation:  
 292 Palaeogeography, Palaeoclimatology, Palaeoecology, v. 261, p. 87–99,  
 293 <https://doi.org/10.1016/j.palaeo.2008.01.009>.  
 294 Moore, T.C., Backman, J., Raffi, I., Nigrini, C., Sanfilippo, A., Pälike, H., and Lyle, M.,  
 295 2004, Paleogene tropical Pacific: Clues to circulation, productivity, and plate motion:  
 296 Paleogeography, v. 19, p. 1–16, <https://doi.org/10.1029/2003PA000998>.  
 297 Moore, T.C., Mitchell, J.N.C., Lyle, M., Backman, J., and Pälike, H., 2007,  
 298 Hydrothermal pits in the biogenic sediments of the equatorial Pacific Ocean:

Geochemistry Geophysics Geosystems, v. 8, p. 1–14,  
<https://doi.org/10.1029/2006GC001501>.

O’Dea, A., et al., 2016, Formation of the Isthmus of Panama: Science Advances, v. 2,  
p. 1–11.

Sun, Q., Wu, S., Hovland, M., Luo, P., Lu, Y., and Qu, T., 2011, The morphologies and  
genesis of mega-pockmarks near the Xisha Uplift, South China Sea: Marine and  
Petroleum Geology, v. 28, p. 1146–1156,  
<https://doi.org/10.1016/j.marpetgeo.2011.03.003>.

Sun, Q., Cartwright, J., Lüdmann, T., Wu, S., and Yao, G., 2017, Three-dimensional  
seismic characterization of a complex sediment drift in the South China Sea:  
Evidence for unsteady flow regime: Sedimentology, v. 64, p. 832–853,  
<https://doi.org/10.1111/sed.12330>.

van Andel, T.H., et al., 1973, Deep Sea Drilling Project Site 157, Initial Reports of the  
Deep Sea Drilling Project, Volume 16: Washington, D.C., U.S. Government Printing  
Office, p. 53–150.

## FIGURE CAPTIONS

Figure 1. A: Geodynamic setting (CNS—Cocos–Nazca spreading center; HS—hotspot).  
B: Map of Carnegie Ridge (grid size = 150 m); conventional bathymetry is in pale color;  
multibeam is dark color. Black dotted lines are areas where dense depressions fields have  
been identified. Thin black lines show ATACAMES cruise (<http://campagnes.flotteoceanographique.fr/campagnes/12010010/>) tracks, along which high-resolution  
multibeam data allow us to recognize polygonal depressions fields (stars).

322

323 Figure 2. Map of studied area (same color scale as that in Fig. 1B). In pale and dark  
324 colors, respectively, multibeam data before (grid size = 150 m) and after (grid size = 50  
325 m) the ATACAMES cruise (<http://campagnes.flotteoceanographique.fr/campagnes/12010010/>). Isocontours = 25 m. Thick black lines show locations of seismic lines on  
326 Figure 4. S—large seamounts. White dotted line shows location of acoustic basement  
327 step; white boxes are locations of Figure 3.

329

330 Figure 3. A–B: Close-ups (zooms) of depressions field (locations in Fig. 2). Red line  
331 shows location of seismic profile ATAC124; white line shows location of seismic zoom2  
332 in Figure 4B.

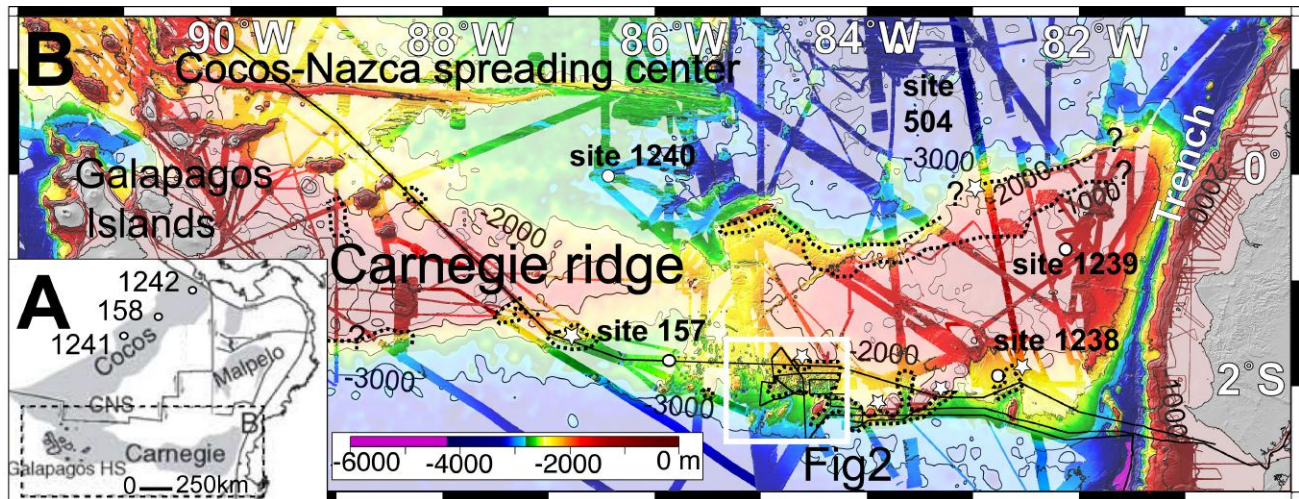
333

334 Figure 4. Seismic profiles (see location in Fig. 2). A: Profiles ATAC130–129 showing  
335 two regional seismic units, u1 and u2. B: Profiles ATAC124–126 crossing depression  
336 field. Dotted blue line is real seafloor depth. Side echoes can appear above seafloor. Red  
337 rectangles are locations of close-ups (zooms); u1—lower unit (u1a—poorly reflective;  
338 u1b—subparallel continuous reflectors); u2—upper unit; VE—vertical exaggeration;  
339 CDP—common depth point.

340

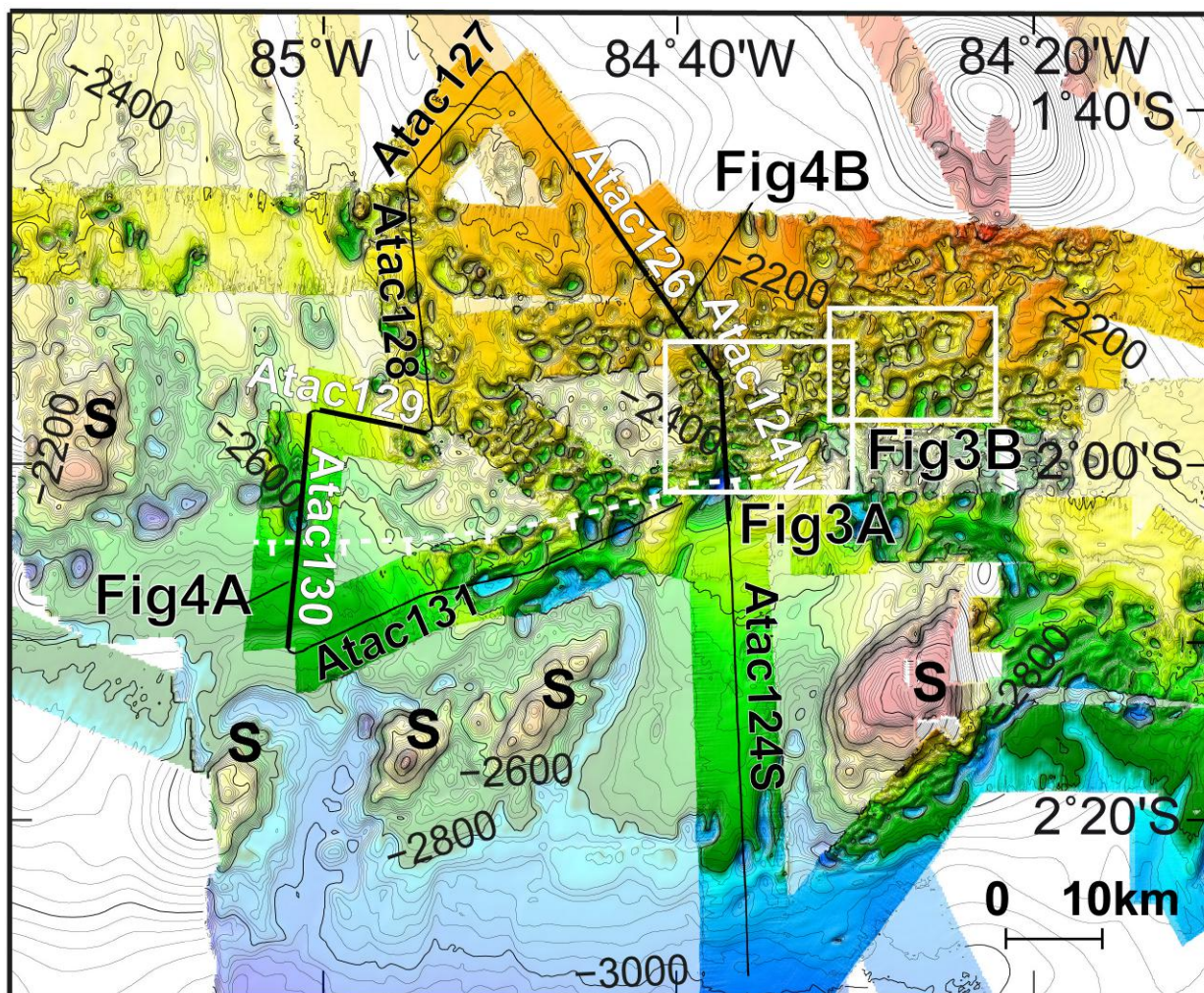
341 Figure 5. Diagram showing two scenarios for origin of honeycomb pattern (HP). A:  
342 Polygonal fault network. B: Pits over basement irregularities at initiation of depressions.  
343 Red circles show final stage of depressions. Red dotted arrows along polygonal faults in  
344 A show bottom current channeled by seafloor furrows formed along fault planes, offering

345 a convergent (c) and divergent (d) geometry every other triple junction. C–F: Successive  
 346 stages of evolution of HP along cross section X–Y; df—diagenetic front. Pockmarks (C)  
 347 and pits (D) formed at seafloor evolve toward larger and deeper subcircular depressions  
 348 (E) in response to scouring action of strong bottom currents on fluid-damaged sediment;  
 349 this stage initiated at the Pliocene-Pleistocene boundary, contemporaneous with closure  
 350 of the Panama Basin, leaving a honeycomb pattern of interdepression ridges. (F) Last, u2  
 351 sediment drift is plastered against the wall of some depressions carved in u1.  
 352



354 FIGURE 1





356 FIGURE 2



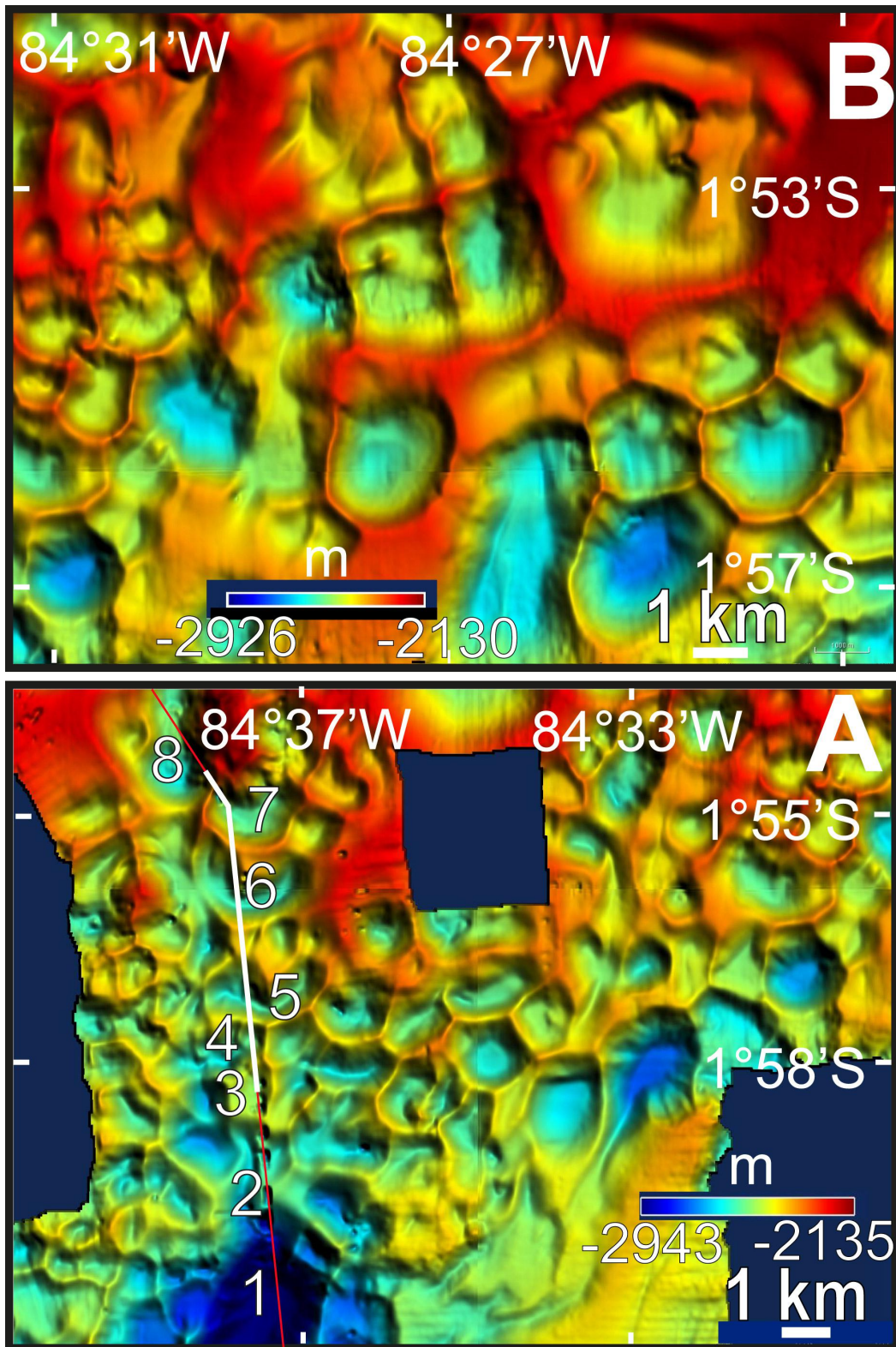
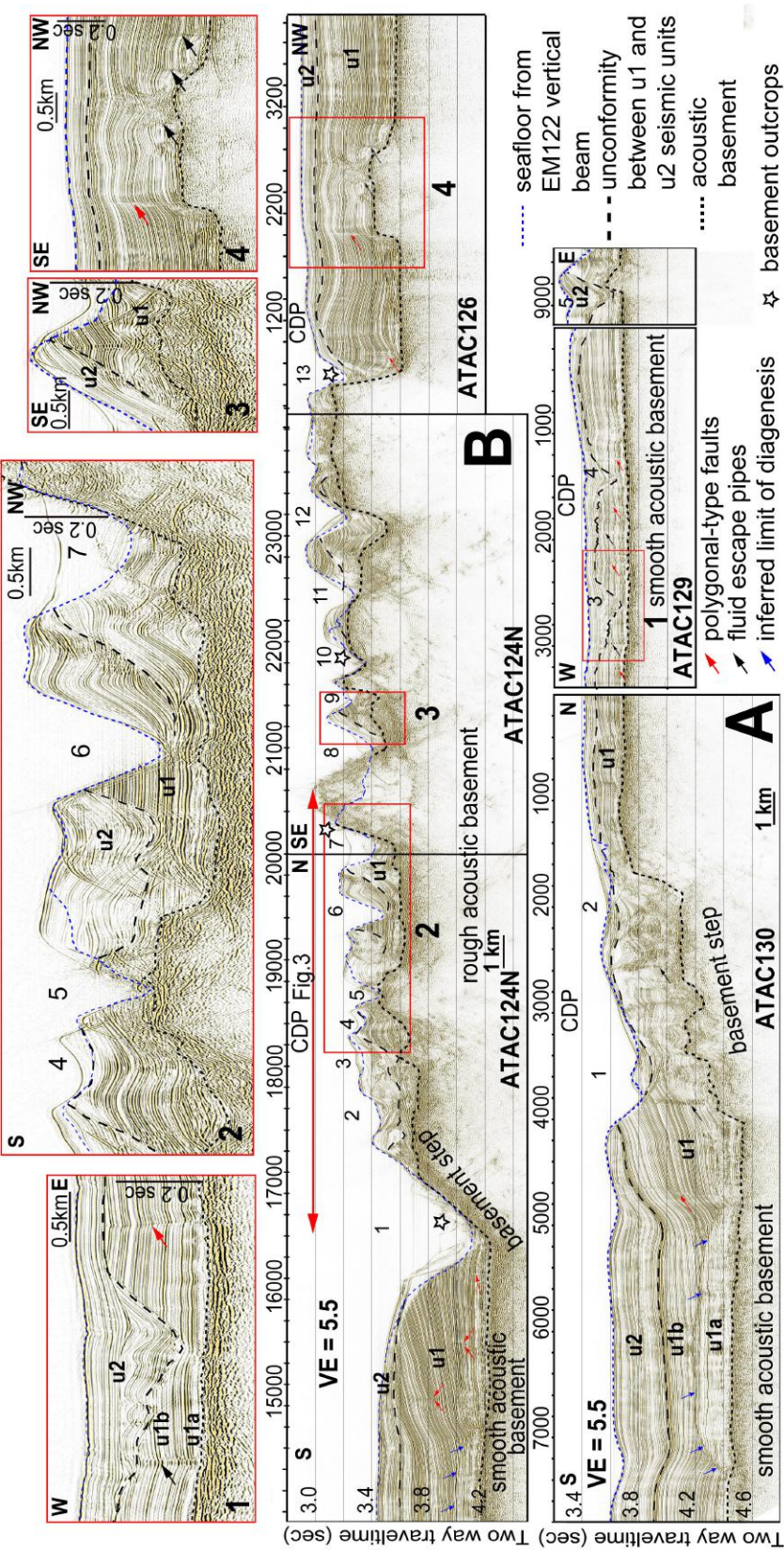


FIGURE 3



359      FIGURE 4



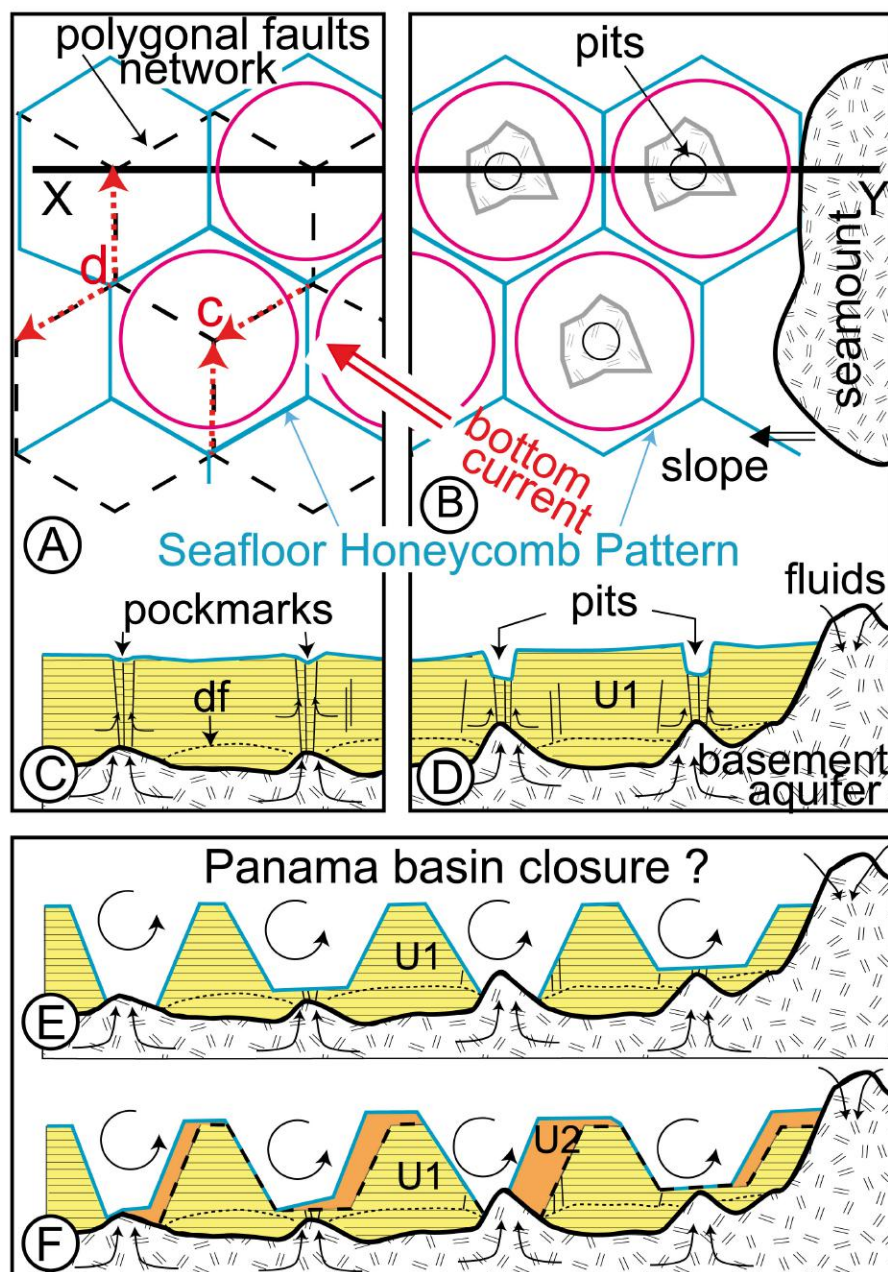


FIGURE 5

<sup>1</sup>GSA Data Repository item 2018392, Table DR1 (correlation with basement irregularities and the morphological parameters of depressions along the seismic profiles), Figure DR1 (correlation between seismic structures, drilled lithologies and ages from DSDP 157), Figure DR2 (swath bathymetry along the southern flank of the Carnegie Ridge), and Figure DR3 (interpretation of the available ATACAMES cruise seismic profiles), is available online at <http://www.geosociety.org/datarepository/2018/> or on request from [editing@geosociety.org](mailto:editing@geosociety.org)

GSA Data Repository 2018392

**A honeycomb seafloor morphology in carbonate sediment of the Carnegie Ridge (offshore Ecuador): Formation and potential geodynamic significance**

F. Michaud<sup>1,2\*</sup>, J.Y. Collot<sup>1</sup>, G. Ratzov<sup>1</sup>, J.N. Proust<sup>3</sup>, A. Dano<sup>1</sup>, J.F. Lebrun<sup>4</sup>, M.J. 4 Hernández<sup>1,5,6</sup>, G. Loayza<sup>7</sup>, A. Khaoulani<sup>1</sup>, Y. Stoll<sup>1</sup>, H. Pouderoux<sup>3</sup>, and L. De Min<sup>4</sup>

<sup>1</sup> *Université Côte d'Azur, IRD (Institut de Recherche pour le Développement), Sorbonne Université, CNRS (Centre National de la Recherche Scientifique), Observatoire de la Côte d'Azur, GEOAZUR (laboratoire de Géoazur), 06560 Valbonne, France*

<sup>2</sup> *Sorbonne Université, Faculté des Sciences et Ingénierie, F-75252 Paris, France*

<sup>3</sup> *CNRS, OSUR (Observatoire des Sciences de l'Univers de Rennes), Géosciences Rennes, Université de Rennes, 35042 Rennes, France*

<sup>4</sup> *Université des Antilles et de la Guyane, Département de Géologie, Pointe à Pitre 97157, France*

<sup>5</sup> *Sorbonne Université, Institut des Sciences de la Terre de Paris (ISTeP), Campus Pierre et Marie Curie, 75252 Paris, France*

<sup>6</sup> *Departamento de Geología, Escuela Politécnica Nacional, Quito, Ecuador*

<sup>7</sup> *Escuela Superior Politécnica del Litoral, Guayaquil, Ecuador*

\*e-mail: [michaud@geoazur.unice.fr](mailto:michaud@geoazur.unice.fr)



**supplemental information**

**Table of contents**

Table DR1: Depressions characteristics along the seismic profiles.

Figure DR1: Correlation between our seismic units (u1, u2, acoustic basement) with a seismic line, drilled lithology and age from the DSDP 157 (from van Andel et al., 1973).

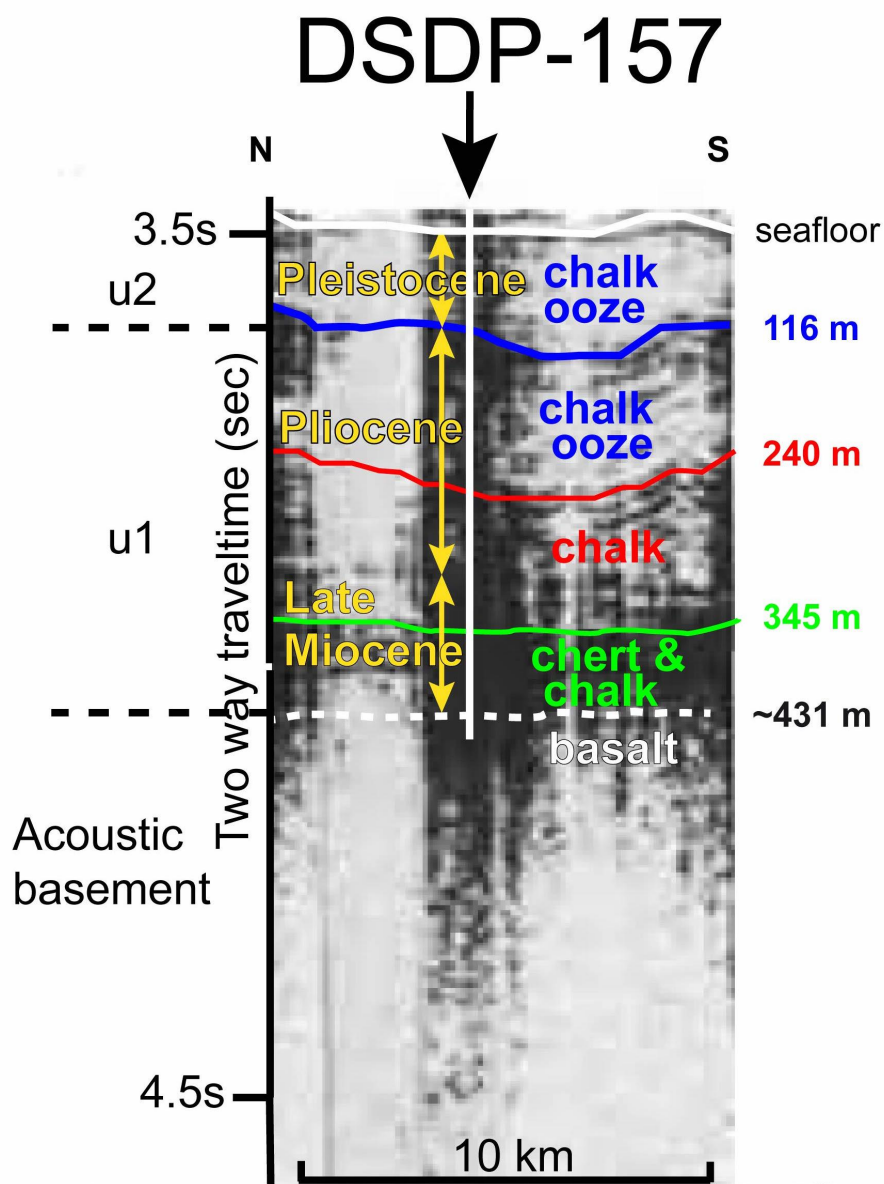
Figure DR2: A) Bathymetric map southeast of the studied area along the southern flank of the Carnegie ridge where high resolution multibeam were recorded during the Atacames cruise B) 3D zoom of the high resolution multibeam, showing honeycomb pattern around the seamounts

Figure DR3: Interpretation of the available seismic profiles (ATAC 131, ATAC 128, ATAC 127 and ATAC 124S, location on Figure 2) in the study area in addition to the seismic profiles of Figure 4.

Depressions characteristics along the seismic profiles					
Seismic Profile Depression number	Depth (m)	Width (km)	Polygonal form	Basement irregularity	Filled by sediments
<b>124S</b>					
1	150	3.9	No	Yes	No
<b>124N-126</b>					
1	475	5.2	No	Yes	No
2	80	1.0	No	No	No
3	30	1.0	Yes	No	No
4	125	0.8	Yes	Yes	No
5	175	0.85	Yes	Yes	No
6	200	1.1	Yes	Yes	Partially
7	200	1.5	Yes	Yes	No
8	250	1.6	Yes	Yes	Partially
9	75	0.8	Yes	Yes	No
10	200	2.0	Yes	Yes	No
11	250	1.2	No	No	No
12	175	1.4	No	Yes	No
13	200	1.3	No	Yes	Partially
<b>130-129</b>					
1	300	3.1	No	Yes	No
2	50	1.2	No	Yes	No
3	"150"	"2"	Unknown	No	Yes
4	"150"	"1"	Unknown	No	Yes
5	"225"	"2"	Unknown	Yes	Yes
<b>131</b>					
1	75	2	No	Yes	No
2	250	3.5	No	No	Partially
3	375	3.0	No	No	No
4	475	3.8	No	Yes	No
<b>128</b>					
1	"275"	"4"	Unknown	Yes	Yes
2	250	4.3	No	Yes	No
3	300	2.0	No	Yes	No
4	125	2.0	No	No	Partially
5	150	1.1	No	Yes	Partially
6	250	1.5	No	Yes	Partially
	30 m to 475m	0.8 km to 5.2 km		73% of depressions related to a basement irregularity	62 % of the depression unfilled

425

426 Table DR1: Depressions characteristics along the seismic profiles. The numbers correspond to the  
427 depressions along the seismic profiles and located on Figure 2,3, 4 and S1). Semi-quantitative  
428 estimation based on all seismic lines crossing the depressions that we have acquired in the area  
429 (figure 2 for line location). Some statistic is done about 1) the link between the basement  
430 roughness and the depression location (73% of depressions are related to a basement irregularity);  
431 and 2) about the sedimentary filling (38% of the depression are filled by u2 sedimentary unit.  
432



**Our interpreted  
units u1 and u2**

**Correlation between seismic structures, drilled  
lithologies, and ages from Van Andel et al., 1973**

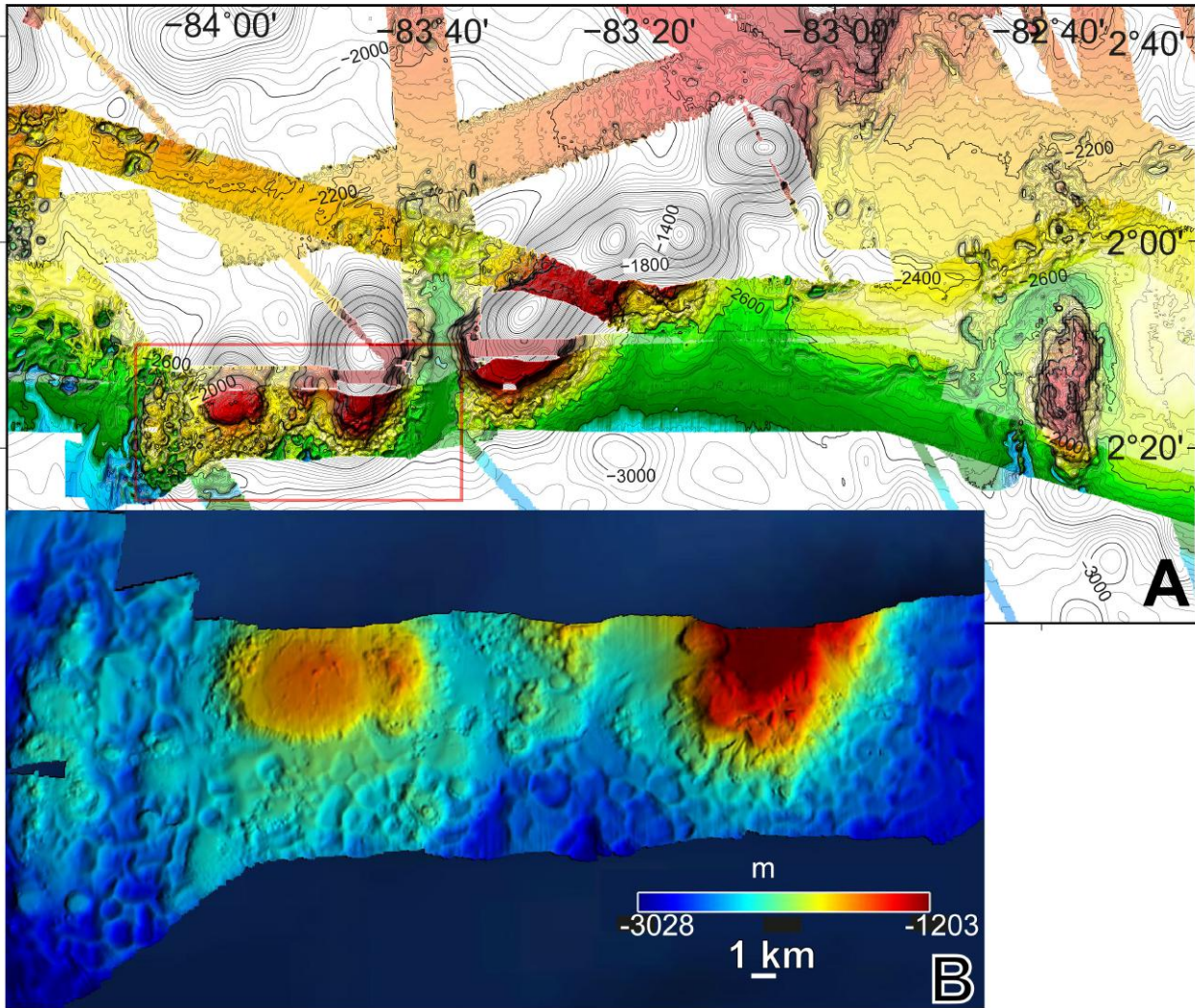
434

435 Figure DR1: Correlation between our seismic units (u1, u2, acoustic basement) with a seismic  
436 line, drilled lithology and age from the DSDP 157 (from Van Andel et al., 1973).

437

438





440

441 Figure DR2: A) Bathymetric map southeast of the studied area along the southern flank of the  
 442 Carnegie ridge where high resolution multibeam were recorded during the Atacames cruise (same  
 443 color scale as that in Fig. 1B and 2). In pale color the multibeam before the Atacames cruise (grid  
 444 size 150m). In dark shade, multibeam from the Atacames cruise (grid size 50m). Iso  
 445 contours=25m. B) 3D zoom high resolution multibeam showing honeycomb pattern around the  
 446 seamounts (location in Fig S2 A). Vertical exaggeration x3. Northward vertical view.  
 447

448



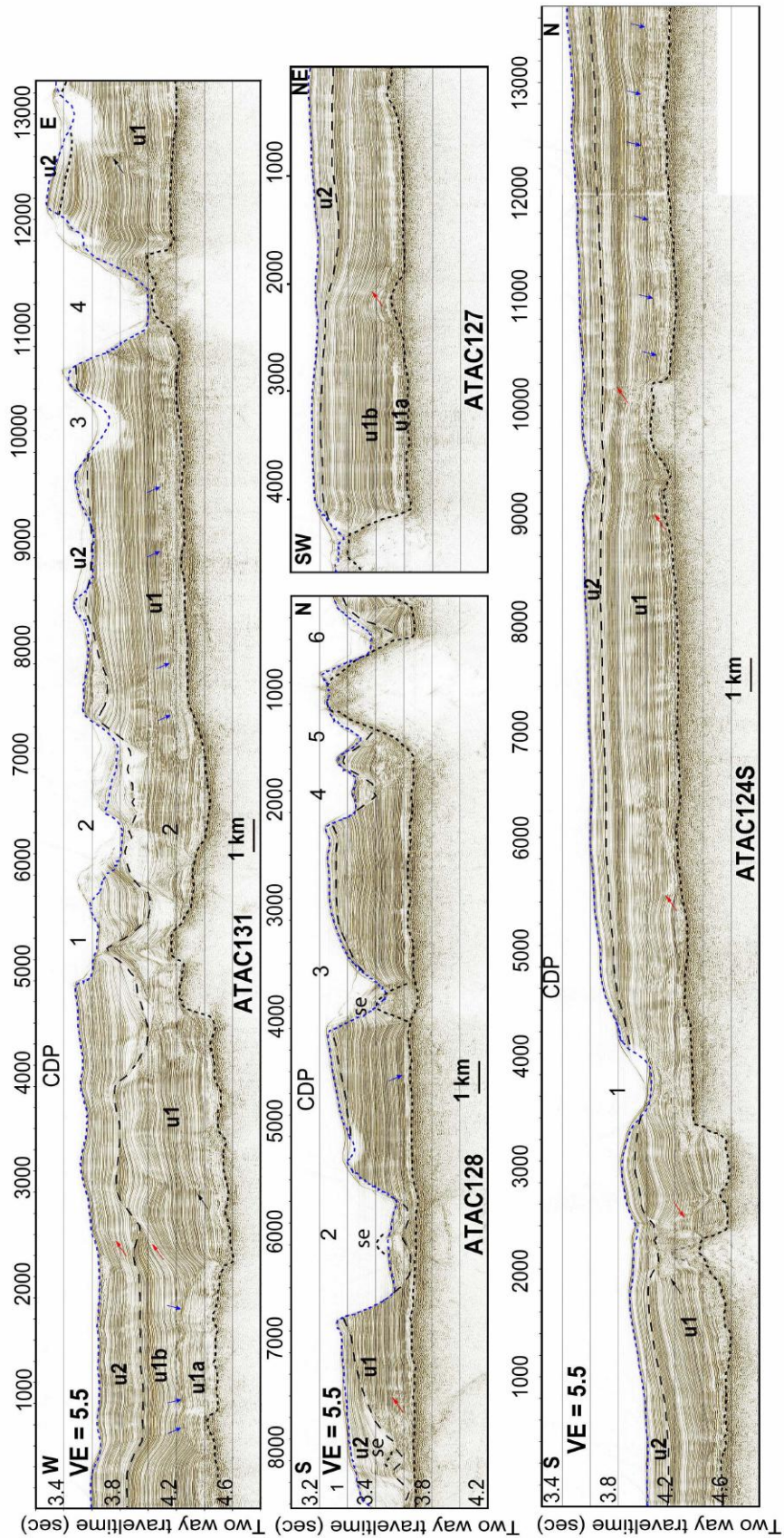


Figure DR3: Interpretation of the available seismic profiles (ATAC 131, ATAC 128, ATAC 127 and ATAC 124S, location on Figure 2) in the study area in addition to the seismic profiles of Figure 4. With this additional figure, all available seismic lines are shown. Short dotted black line=acoustic basement; large dotted black line=unconformity between lower and upper seismic units; blue arrows=inferred upper limit of diagenesis and lithification; red rectangle=location of the zooms; u1=lower unit (u1a=poorly reflective; u1b = sub parallel continuous reflectors); u2=upper unit. Se = Side echo related to possible irregularities of the basement. Numbers correspond to the depressions considered in the table 1. Dotted blue line = seafloor depth EM122 vertical beam allows to discriminate side echoes figured above the seafloor.